Journal Pre-proofs

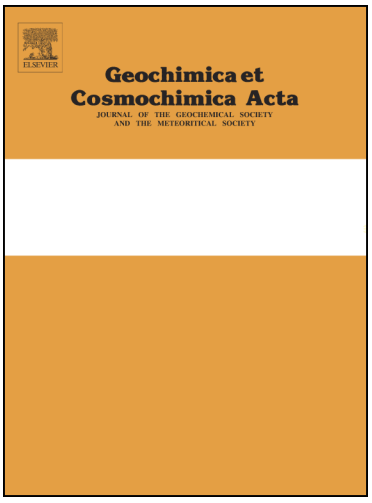

Low source-inherited iron solubility limits fertilization potential of South American dust

Lucio E. Simonella, Nicolás J. Cosentino, María L. Montes, Peter L. Croot, Miriam E. Palomeque, Diego M. Gaiero

PII: S0016-7037(22)00320-9
DOI: https://doi.org/10.1016/j.gca.2022.06.032
Reference: GCA 12696

To appear in: *Geochimica et Cosmochimica Acta*

Received Date: 24 December 2021
Revised Date: 19 May 2022
Accepted Date: 23 June 2022

Please cite this article as: Simonella, L.E., Cosentino, N.J., Montes, M.L., Croot, P.L., Palomeque, M.E., Gaiero, D.M., Low source-inherited iron solubility limits fertilization potential of South American dust, *Geochimica et Cosmochimica Acta* (2022), doi: https://doi.org/10.1016/j.gca.2022.06.032

Low source-inherited iron solubility limits fertilization potential of South American dust

Lucio E. Simonella[1], Nicolás J. Cosentino[2], María L. Montes[3,4], Peter L. Croot[5], Miriam E. Palomeque[6], and Diego M. Gaiero[6,7]

[1]Facultad de Ciencias Químicas, Universidad Nacional de Córdoba. Av. Medina Allende y Haya de la Torre, Córdoba, Córdoba, Argentina.

[2]Instituto de Geografía, Facultad de Historia, Geografía y Ciencia Política, Pontificia Universidad Católica de Chile. Av. Vicuña Makenna 4860, Macul, Región Metropolitana, Chile.

[3]Consejo Nacional de Investigaciones Científicas y Tecnológicas (CONICET), Instituto de Física La Plata (IFLP), Universidad Nacional de La Plata. Diagonal 113 entre 63 y 64, La Plata, Prov. de Buenos Aires, Argentina.

[4]Facultad de Ciencias Exactas, Universidad Nacional de La Plata. Calle 115 y 47, La Plata, Prov. de Buenos Aires, Argentina.

[5]Irish Centre for Research in Applied Geoscience (iCRAG), Earth and Ocean Sciences, School of Natural Sciences and Ryan Institute, National University of Ireland Galway. O'Brien Centre for Science (East), University College Dublin, Belfield, Dublin 4, Ireland.

[6]Facultad de Ciencias Exactas, Físicas y Naturales, Universidad Nacional de Córdoba. Av. Vélez Sársfield 1601, Córdoba, Córdoba, Argentina.

[7]Consejo Nacional de Investigaciones Científicas y Tecnológicas (CONICET), Centro de Investigaciones en Ciencias de la Tierra (CICTERRA), Universidad Nacional de Córdoba. Av. Vélez Sársfield 1699, Córdoba, Córdoba, Argentina.

Authors' emails (*corresponding): LES (lsimonella@unc.edu.ar), NJC (nicolas.cosentino@uc.cl), MLM (lmontes@fisica.unlp.edu.ar), PLC (peter.croot@nuigalway.ie), MEP (mirpalomeque@unc.edu.ar) and DMG* (diego.gaiero@unc.edu.ar)

Abstract

Where atmospheric processing is weak due to low anthropogenic emissions, fertilization of iron-limited oceans by non-volcanic mineral dust aerosols strongly depends on iron solubility at the sources. Southern South America (SSA) is a pristine environment and the main dust supplier to the southern oceans, the most sensitive to iron fertilization. Thus, the present-day lack of SSA dust fertilization of the southern oceans is hypothesized to reflect low source-inherited iron bioavailability. However, a dearth of geochemical studies on SSA dust prevents testing this hypothesis. To remedy this, we conducted the first systematic sampling of SSA dust sources. Iron leaching experiments showed fractional solubilities of close-to-source dust (bulk) and dust-emitting surface sediments (<63 μm) in pure water (0.05 ± 0.05%), seawater (0.03 ± 0.04%) and 1% nitric acid (5 ± 6%) that imply a low mass-normalized fertilization potential of SSA dust compared to dust from other regions. Based on grain size, size-resolved mineralogy, elemental chemistry and iron speciation determinations, we found that variability in labile iron is enhanced by high clay contents, small grain size and higher proportions of paramagnetic versus non-paramagnetic iron, irrespective of oxidation state. The independence of the most labile, water-soluble iron on grain size and its strong negative correlation to the Chemical Index of Alteration may imply that we currently underestimate the role of coarse glaciogenic dust as a supplier of bioavailable iron during drier-than-present ice ages when continental chemical weathering was reduced, and during which enhanced supply of dust-borne bioavailable iron to the southern oceans is observed.

1 Introduction

Mineral dust aerosols have the potential to alleviate Fe limitation of primary productivity in high-nutrient, low-chlorophyll (HNLC) oceans, thus impacting global climate through enhanced

atmospheric CO_2 sequestration (Martin, 1990; Moore et al., 2001). This mechanism, coupled with export of organic C to the deep ocean, has been proposed to contribute to millennial-scale global changes in atmospheric pCO_2 (Martin, 1990). The oceans south of 34ºS are the most sensitive to Fe fertilization (Lambert et al., 2021), and southern South America (SSA) has been its main contributor of non-volcanic (i.e., not associated to primary ashfall) mineral dust aerosols (henceforth *dust*) since the last glacial period, particularly to the Atlantic sector (Li et al., 2008; Neff and Bertler, 2015; Gili et al., 2017; Kok et al., 2021). However, available evidence suggests that SSA dust has no effect on primary producers' biomass in the present-day climate (Meskhidze et al., 2007; Johnson et al., 2011; Cosentino et al., 2020a). Thus, to shed light on how this mechanism may have operated in the past, it is key to understand the reasons for this present-day lack of response of southern oceans' productivity to SSA dust.

While volcanic ash has been shown to fertilize the Atlantic (Browning et al., 2014) and Pacific (Vergara-Jara et al., 2021) sectors of the southern oceans, available evidence favors the interpretation that dust does not have such an effect. The first studies that proposed a fertilizing effect of dust in the Atlantic sector of the southern oceans were based on correlations of modeled dust deposition fields and satellite chlorophyll-a concentration ([Chl-a], Erickson III et al., 2003) or net community production measurements (Cassar et al., 2007). Instead, Meskhidze et al. (2007) attributed such correlations to an atmospheric circulation pattern that simultaneously uplifts Patagonian dust and upwells nutrient-rich waters. In line with this interpretation, no satellite evidence of dust-related [Chl-a] enhancement was found in studies that looked at individual dust outbreaks from two regions in northern (Johnson et al., 2011) and southern (Cosentino et al., 2020a) Patagonia.

The main factors that influence dust-borne Fe bioavailability include ocean biogeochemistry, light availability, atmospheric processing and source physical and chemical characteristics. Dust emissions in southern and central-western SSA are concentrated during austral spring and summer (Gaiero et al., 2003; Crespi-Abril et al., 2018; Gassó and Torres, 2019; Cosentino et al., 2020a, 2021), when no light limitation exists. Based on limited measurements (World Ocean Atlas 2018) and biogeochemical modeling (Song et al., 2016), summertime outer Patagonian shelf and proximal open ocean waters are found to be HNLC, and its primary productivity limited by Fe, possibly co-limited by Si (Cosentino et al., 2020a). Limitation by Fe was confirmed in the northern Drake Passage, close to the South American continental shelf, based on in-situ incubation experiments (Browning et al., 2021). Instead, further south in the central Drake Passage limitation by Mn as well as Fe-Mn co-limitation were identified (Browning et al., 2021). Further downwind of SSA, the southern oceans are markedly HNLC (Martin et al., 1990). No direct measurements exist of atmospheric acidity downwind of Patagonia, although relatively low (vs. global) modeled cloud condensation nuclei suggests pristine conditions (Hamilton et al., 2014). Regional dust cycle models showed that soluble dust Fe delivery to the South Atlantic Ocean is more sensitive to changes in source-inherited soluble Fe than in the degree of atmospheric processing (Johnson et al., 2011). Characterization of dust sources in SSA is thus key to understanding the lack of present-day dust fertilization in the southern oceans (Shoenfelt et al., 2017; Cosentino et al., 2020a).

Dust sources in SSA were first systematically identified by Prospero et al. (2002) based on the Total Ozone Mapping Spectrometer (Figure 1). They are concentrated in arid and semi-arid landscapes of the South American Arid Diagonal (SAAD), a SE-NW-oriented regional land belt characterized by hydrologic deficit (i.e., total evaporation higher than total precipitation) or

reduced positive water balance. The main sources are, from north to south, the Puna-Altiplano Plateau (PAP), central-western Argentina (CWA), Patagonia and Tierra del Fuego (TdF). The PAP is a high-elevation (~4000 meters above sea level) basin in the central Andes with numerous endorheic depocenters. Present-day dust is emitted from the edges of salar pans within these depocenters, which are the remnants of Pleistocene paleo-lakes, as well as from adjacent alluvial fans (Prospero et al., 2002; Placzek et al., 2011; Gaiero et al., 2013). In CWA, a series of W-E ephemeral rivers and streams derived from the Andes reach the eastern foothills and form alluvial fans and playa lakes (Gili et al., 2017), from where persistent dust emissions take place (Mingari et al., 2017). Dust sources in Patagonia and TdF are concentrated in eastern Patagonia/TdF. They mostly consist of non-glaciogenic sources such as the non-consolidated surfaces of dry lake Colhué Huapi (Montes et al., 2017; Gassó and Torres, 2019) and numerous ephemeral small lakes formed in deflation pans (Gassó and Stein, 2007; Gassó et al., 2010; Villarreal and Coronato, 2017; Cosentino et al., 2020a, 2021). Much less relevant in terms of surface area and emission intensity are armored and unarmored alluvial deposits of glacial origin in ephemeral, incised outwash plains (Hernández et al., 2008).

The main objective of this study is to gauge the fertilization potential of present-day SSA dust. We do so by quantifying the degree to which Fe in dust-emitting surface sediments and in wind-borne dust collected close to the sources solubilizes in a set of solutions (i.e., pure water, 1% nitric acid and seawater), and by comparing against a global data set of similar observations. Another objective is to determine the main controls on Fe solubility, which we assess by characterizing samples in terms of a set of physical and chemical properties. Our final objective is to explore the possible implications of our results on the potential biogeochemical impacts of SSA dust during glacial times. We do so by speculating on how the identified controls on

present-day Fe solubility of SSA dust and dust-emitting surface sediments may have operated during past glacial periods.

2 Materials and methods

2.1 Sampling

Dust samples were obtained from six monitoring stations spanning SSA between 25-54ºS (Figure 1, Table S1). Five stations are located in regions of intense dust activity within the SAAD: three in continental Patagonia (Cosentino et al., 2021), one on the island of TdF (Cosentino et al., 2020a) and one in the PAP. The remaining station is located east of CWA, in the loessic Pampean region (Cosentino et al., 2020b). These stations are installed on the outskirts of cities, with few to no buildings and roads nearby, and are equipped with three passive traps: one Capteur Pyramidal (CP, Orange et al., 1990), one Big Spring Number Eight (BSNE, Fryrear, 1986) and one Modified Wilson And Cook (MWAC, Wilson and Cooke, 1980), all placed 5 meters above ground level to avoid collecting local saltation particles (Figure S1). These traps accumulate material during average sampling periods of 12-38 days depending on the station, after which an operator collects the samples using a vacuum pump to filter particles on a previously weighted 0.45-μm membrane.

We also sampled ~500 g of loose surface (i.e., upper 5 cm) sediments of previously identified dust-emitting surfaces (Gaiero et al., 2013; Gili et al., 2017; Cosentino et al., 2020a, 2021) at 21 locations across the SAAD (Figure 1) using polythene sample bags and plastic scoops. These surfaces consisted of exposed lake beds from ephemeral lakes, alluvial deposits in ephemeral, incised outwash plains, alluvial fans in intermontane closed basins and salar pans (Figure S2).

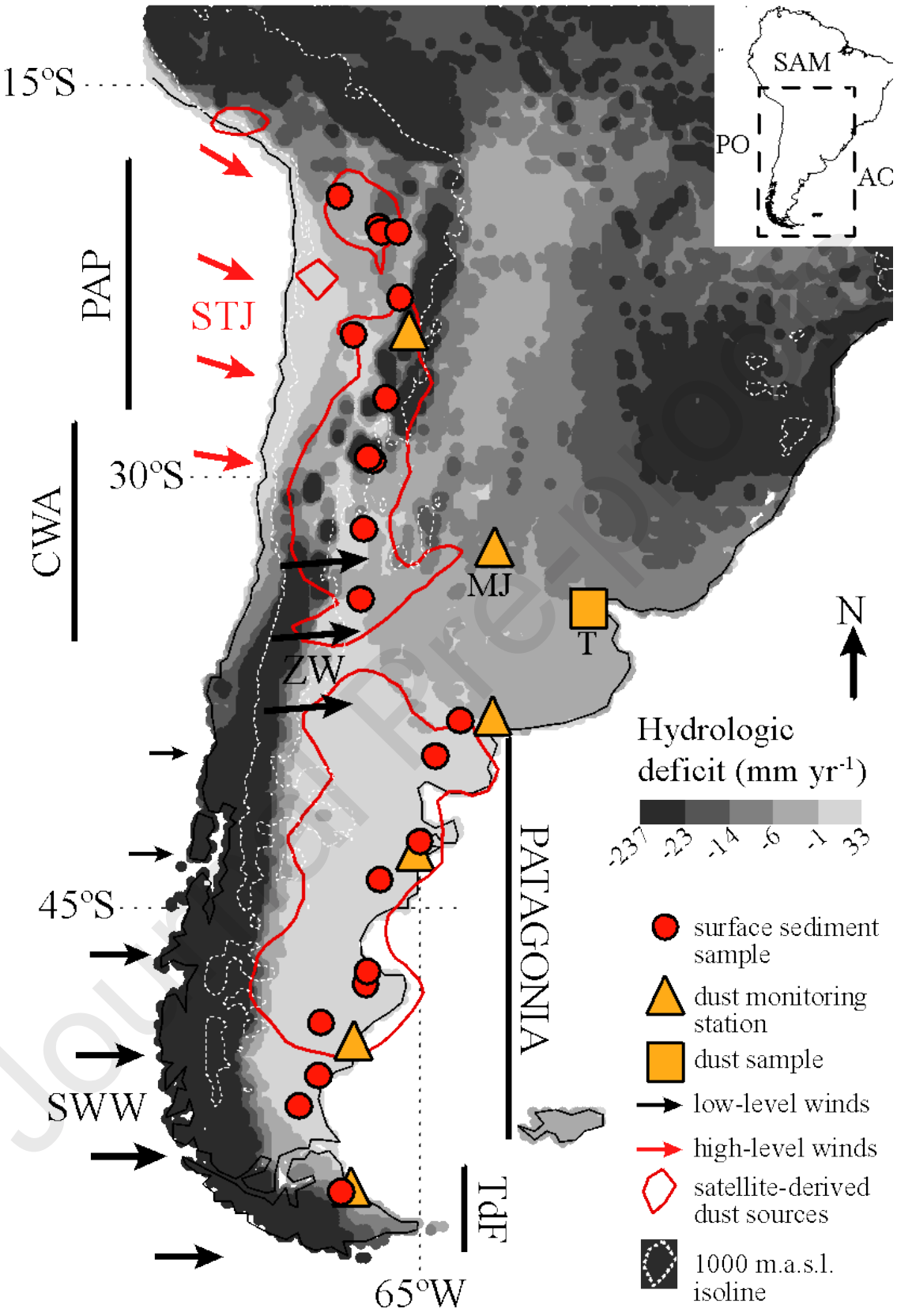

Figure 1. The South American Arid Diagonal. Dust contours indicate areas where the absorbing aerosol index derived from the Total Ozone Mapping Spectrometer was ≥0.7 during ≥7 days per month, for a 1980-1992 climatology (Prospero et al., 2002). Hydrologic deficit is calculated as total evaporation minus total precipitation, which were derived from monthly ERA5-Land reanalysis data between 1981-1992. The 1000-meter above sea level (m.a.s.l.) isoline corresponds to the 0.25º lat-lon resolution TerrainBase dataset. TdF: Tierra del Fuego, CWA: Central Western Argentina, PAP: Puna-Altiplano Plateau, MJ: Marcos Juárez, T: Temperley, SAM: South AMerica, PO: Pacific Ocean, AO: Atlantic Ocean, SWW: South Westerly Winds, ZW: Zonda Winds, STJ: SubTropical Jet.

2.2 Sieving and laser diffraction

With the objective of physically and chemically characterizing the fraction of surface sediments subject to deflation and atmospheric transport, surface sediment samples were previously dry-sieved using two plastic meshes of 63 μm and 11 μm sizes. The Stokes method was used to separate the <5-μm fraction. In total, three grain size fractions were obtained for surface sediment samples: 0-63 μm, 0-11 μm and 0-5 μm. Concerning dust samples, only bulk samples were analyzed due to typically low masses available.

Grain size distributions (GSD) of bulk dust and <63-μm surface sediment samples were measured by laser diffraction (Horiba LA-950, range: 0.01-3000 μm). The reproducibility of measurements was tested using mixtures of glass beads (NIST Traceable polydisperse particle standard PS202/3–30 μm and PS215/10–100 μm, Whitehouse Scientific). The two standard runs (PS202, n = 6 and PS215, n = 5) resulted in median (D50) and D10/D90 percentiles within 3% and 5% of the certified nominal values, respectively.

2.3 X-ray diffraction

The mineralogical composition of bulk dust samples and of the three grain size fractions of surface sediment samples (<63 μm, <11 μm and <5 μm) was determined based on powder X-ray

diffraction (XRD, PANalytical X'Pert Pro), under standard radiation conditions (CuKα, 1.54060 Å, 40 kV, 40 mA, Bragg-Brentano geometry). In all cases it was ensured that samples were not preferentially oriented to avoid the overestimation of non-equiaxed minerals. A stepwise scanning procedure was employed (0.02º, 1 s, 2θ range: 5-72º). Diffractogram fitting was performed using the X'Pert HighScore software (Figure S3). First, a list of minerals identified based on diagnostic peaks on at least one sample was obtained: quartz, K-feldspar, plagioclase, calcite, clays, amphibole, chlorite, halite, gypsum, hematite and pyrophyllite. Next, the intensities of the reflections of each mineral in each sample were multiplied by a semi-quantification factor specific for each mineral (Cook et al., 1975; Boski et al., 1998). Finally, the proportions of each identified mineral in the full sample set were calculated for each sample.

2.4 Leaching experiments

The release of Fe in dust (bulk) and surface sediment (<63-µm and <11-µm fractions) samples was evaluated with a continuous flow method, which is described in full and validated in Simonella et al. (2014). Briefly, a solution extraction stream was propelled by a peristaltic pump (Gilson Minipuls 3) at 1.0 mL min^{-1} through a column that contained ~5 mg of the sample, ran in triplicates, as well as a methodological blank (i.e., no sample). First, deionized water (Milli-Q, pH ~ 5) passed through the column for 20 min. This step is intended to measure soluble Fe in the most labile mineral phases, mimicking Fe release under slightly acidic, natural rainwater (Fe_{MQ}). We consider this most labile Fe to be the source-inherited soluble Fe in dust, not enhanced by either wet or dry post-emission atmospheric processing. The second step consisted of extraction with a diluted acid solution (sub-boiled 1% v/v HNO_3, pH ~ 2) for 2 h. This is intended to measure Fe in less labile, water-insoluble mineral phases in dust. This Fe (Fe_{AC}) is potentially released during the many possible dry and wet mechanisms acting on dust particles within the

atmosphere to enhance soluble Fe (i.e., atmospheric processing), and/or during post-depositional mechanisms within the surface ocean. We argue that Fe_{AC} represents an upper bound to soluble Fe due to any combination of these mechanisms of post-emission soluble Fe enhancement (e.g., Cosentino et al., 2020a). We define labile Fe as total Fe released after these two steps (Fe_{MQ} + Fe_{AC}), following the nomenclature of Perron et al. (2020). The solid-to-liquid ratio after the conclusion of the 1%-nitric-acid experiments was 42 mg L^{-1}, which is within the range observed in in-cloud processing (Shi et al., 2012). Solution aliquots were retrieved for seven and 12 sub-steps during the deionized water and acid leaching steps, respectively, collected in acid-washed tubes and their Fe concentration determined in an autosampler-equipped graphite furnace atomic absorption spectrometer (GFAAS, Buck 210). Results varied ± 6% with respect to certified values for the two stages of extraction (reference material: BCR-701).

Iron leaching experiments were also performed on seawater (Fe_{SW}) to measure soluble Fe that could potentially be bioavailable after dry deposition to the ocean and with no previous atmospheric processing (Duggen et al., 2007; Olgun et al., 2011). Surface seawater was sampled ~500 m off the Patagonian coast (42.65ºS, 64.23ºW), filtered in situ with 0.45-µm membranes and stored at 4ºC in acid-washed dark polyethylene bottles. Approximately 10 mg of sample was added to 20 mL of seawater, and cathodic stripping voltammetry (CSV) measurements were performed every few minutes under clean laboratory conditions (Croot and Johansson, 2000). GEOTRACES protocols were followed throughout the experiments, including the use of CRM Arizona test dust as a standard reference material (Cutter et al., 2010). Total measurement time was between 60-230 min.

2.5 Elemental chemistry

The Fe content of bulk dust and each surface sediment size fraction (Fe_{TOT}) was determined by alkaline fusion at 1050ºC using $Li_2B_4O_7$, followed by dissolution in HNO_3, and analysis by inductively coupled plasma-atomic emission spectrometry (Actlabs, Canada). This analysis was performed on subsamples not previously subjected to the two-step leaching process, that is, they constitute total iron (single digestion) as defined by Perron et al. (2020).

The Al, Ca, Na and K concentrations were also determined for the <63-µm fraction of surface sediments to calculate the Chemical Index of Alteration (CIA, Nesbitt and Young, 1982), a measure of the time-integrated intensity of chemical weathering and a proxy for climate change during glacial-interglacial transitions (Wang et al., 2020). The CIA was calculated as CIA = 100 $[Al_2O_3/(Al_2O_3 + CaO^* + Na_2O + K_2O)]$, where CaO* represents silicate calcium, based on the methodology in McLennan (1993).

The detection limit for element determinations was 0.01%, the uncertainty of measurements was 3% (based on 1σ of replicates), and standards NIST 694, NIST 1633b, DNC-1, GBW 07113, W-2a and SY-4 were run simultaneously to check the validity of the results. Measurements of Fe, Al, Ca, Na and K for these standards deviated in average 3% from certified values.

2.6 Mössbauer spectroscopy

Mössbauer spectroscopy was performed on 15 surface sediment samples (<63-µm fraction) to obtain information on Fe speciation, that is, its oxidation state and bonding environment. The resonant nuclear transition of ^{57}Fe at 14.1 keV was used, which allows detection and measurement of sesquioxides and other Fe-bearing minerals such as oxides, hydroxides, oxi-hydroxides and clay minerals. Approximately 300 mg of sample was placed on a plastic container. Measurements were done at room temperature with a conventional spectrometer with

512 channels and constant acceleration. The spectrometer's source consisted of ^{57}CoRh with a nominal activity of ~5 mCi. The velocity calibration was performed with a 12-μm-thick α-Fe foil. The Mössbauer spectra were numerically analyzed using quadrupole splitting distributions. The relative spectral area of each Fe phase allows their semi-quantification (Figure S4). The oxidation state of Fe was determined by analyzing the magnitude of the isomeric shifts (Murad, 2010).

3 Results

3.1 Grain size

The distribution of optical diameters of grains of bulk dust samples is predominantly unimodal with a median between 10-27 μm, except for a dust sample in southern Patagonia at 49.3ºS with a median of 67.5 μm (Table 1, Table S2). In turn, the <63-μm fraction of surface sediments are generally coarser, with unimodal to bimodal distributions with a median between 7-60 μm. As with iron solubility data, no apparent regional trends can be discerned. Within Patagonia though, surface sediments associated with ephemeral or dry lakes are distinctly finer grained (median: 25 ± 16 μm, 1σ) than those associated with topsoils developed on the Patagonian plains (median: 50 ± 9 μm, 1σ). Likewise, the finest grained surface sediment sample from CWA (SCOA9, median: 11.1 μm) and PAP (SPU5, median: 8.1 μm) correspond to the only dry/playa lake sample obtained from each of these regions, compared to respective medians of 42 ± 8 μm (1σ) and 24 ± 12 μm (1σ) for surface sediments in alluvial fan or salar edge depositional environments.

Table 1. Iron speciation, grain size and Chemical Index of Alteration (CIA) of dust and sediment samples.

sample name	paramagnetic $Fe^{2+}/(Fe^{2+}+Fe^{3+})$ (%)[1]	optical diameter, modes (main, secondary, etc.) (μm)[2]	optical diameter, median (μm)[2]	CIA[4]
Puna-Altiplano Plateau				

SAB1	33±4	59.0±0.0, 15.2±0.0	42.5±1.6	45
SAB2	27±3	13.2±0.0	15.4±0.8	55
SAB3	17±2	51.9±9.9	26.9±9.3	50
SAB4	nd	13.2±0.0	16.2±1.3	50
SPU5	43±2	8.9±1.0	8.1±0.6	67
S13	nd	11.2	10.5	nd
SPU6	nd	17.4±0.0	21.1±0.4	62
SPU7	44±4	44.9±0.0	35.7±0.1	58
Central Western Argentina				
SCOA8	nd	51.5±0.0	39.3±0.6	59
SCOA9	34±3	11.6±0.0	11.1±0.1	64
SCOA10	42±4	51.5±0.1	34.6±1.5	60
SCOA11	49±3	59.0±0.0	50.9±0.3	59
Pampean plains (east of South American Arid Diagonal)				
Temperley	nd	15.2	13.7	nd
Patagonia				
SPA12	44±3	77.3±0.0, 11.6±0.0	60.2±0.5	64
SPA13	nd	47.1±3.8	36.5±1.0	42
SPA14	19±2	7.8±0.0	6.6±0.2	68
TW10	nd	19.9, 200	17.4	nd
SPA15	40±5	20.0±21.5, 30.6±15.0	14.5±8.8	61
SPA16	nd	51.5±0.0	42.5±1.0	62
SPA17	52±3	51.5±0.0	31.2±2.1	55
SPA18	24±2	11.6±0.0, 246±24	11.6±0.8	61
SJ16-BSNE	nd	77.3, 13.2	67.1	nd
SPA19	nd	70.8±5.7, 14.5±1.1	51.0±2.6	59
SPA20	35±4	59.0±0.0	47.3±1.4	60
SPA21	79±5	44.9, 10.1	25.5	54
RG13	nd	17.4±0.0	16.0±0.8	nd
RG75[3]	nd	11.6±0.0	10.1±0.3	nd
RG82[3]	19	36.7±3.5	27.0±1.0	nd
RG89-BSNE[3]	nd	24.5±2.3	18.2±0.7	nd
RG89-CP[3]	16	13.2±0.0	11.9±0.4	nd
RG104[3]	13-22	13.2±0.0, 262±0, 0.3±0.0	12.6±0.2	nd

[1]Of the <63 μm fraction. Error is 1σ.

[2]Of the <63 μm fraction in topsoils, and of bulk sample in dust. Errors are 1σ based on 2-4 measurements of the same sample.

[3]Cosentino et al. (2020a). Surface Fe speciation of these dust samples (CP

collector) is based on X-ray photoelectron spectrometry. Total Fe ratio reported (i.e., paramagnetic plus non-paramagnetic).

[4]Of the <63-μm fraction.

nd: not determined

3.2 Iron solubility

Surface sediments (<63 μm)' Fe_{TOT} is similar across the SAAD: 36 ± 11 mg g^{-1} (1σ, Figure 2, Table S3). It is also similar across different grain size fractions: 34 ± 12 mg g^{-1} (<11 μm) and 40 ± 19 mg g^{-1} (<5 μm). The only appreciable regional difference is within the PAP: low values in the Altiplano plateau and high values in the Puna plateau. No evident trends are present with respect to the geomorphological environment of the samples. Dust (bulk) has similar values of Fe_{TOT} content across the SAAD: 41 ± 14 mg g^{-1}, with no regional differences (Figure 2, Table S3). There is high temporal variability in Fe_{TOT} for dust samples collected in the southernmost Patagonian (~130% for six samples collected in a span of 14 years) and Pampean plains (~120% for two samples collected one month apart) monitoring stations.

Mean Fe_{MQ} for dust (bulk) and surface sediments (<63 μm) is 19 ± 13 μg g^{-1} (1σ, range: 2-53 μg g^{-1}), with no distinction between both types of samples (Figure 2a). Mean fractional Fe solubility (FFS) in Milli-Q water (FFS_{MQ}) is 0.05 ± 0.05% (range: 0.007-0.2%, Figure 2a). Mean Fe_{AC} is about two orders of magnitude higher than Fe_{MQ} at 1527 ± 1035 μg g^{-1} (range: 291-4131 μg g^{-1}, Figure 2b). In this case, the difference in solubilities between surface sediment and dust samples is substantial, with values of 1178 ± 1002 μg g^{-1} for surface sediments and almost double at 2017 ± 784 μg g^{-1} for dust samples. However, FFS in the acidic solution (FFS_{AC}) is similar within uncertainty between both types of samples: 4 ± 5% for surface sediments and 6 ± 3% for dust. Labile Fe is thus dominated by the more refractory fraction of Fe that is water-insoluble but

soluble at a pH of 2 (i.e., 99%). Fe_{SW} for two surface sediment and 17 dust samples is similar to Fe_{MQ}, with a mean value of 15 ± 18 μg g^{-1} (range: 0.1-66 μg g^{-1}), and FFS in seawater (FFS_{SW}) for 15 of those samples of 0.03 ± 0.04% (range: 0.0003-0.12%, Figure 2c). No regional trends are discernible.

We compare the time it takes to dissolve Fe from each sample by defining a single scalar index as $T_{Fe\_sol} = (t_{25\%} + t_{50\%} + t_{75\%})/3$, where t_i is the time after which percentage i of the maximum (i.e., final) concentration of Fe measured during the leaching experiments is attained. While this is an index with units of time, the fact that it measures times of dissolution to a given percentage of each sample's final concentration implies that the index contains information on the rate of Fe dissolution in each sample. While using a single index to characterize the rate of Fe dissolution is a simplification of a behavior characterized in similar samples by a fast initial release followed by a more protracted release (e.g., Simonella et al., 2014), this index may be used to easily compare average dissolution rate between samples. Iron dissolution in deionized water is faster for the <63-μm fraction (T_{Fe_sol} = 5 ± 2 min, 1σ) than for the <11-μm fraction (8 ± 3 min) of dust-emitting surface sediments and bulk dust (8 ± 1 min) across the SAAD (Table 2). In contrast, Fe dissolution in acid solution is 5-8 times slower (T_{Fe_sol} = ~39-41 min). The index of Fe dissolution velocity of bulk dust samples in seawater (T_{Fe_sol} = 32 ± 18 min) is closer to that of bulk dust in acid solution (39 ± 2 min) than in deionized water. This difference in mean dissolution speed reflects differences in the labile Fe pool available under different extraction schemes (i.e., Milli-Q vs. acid vs. seawater). Within each extraction scheme and grain size range, there are no appreciable regional differences in T_{Fe_sol}.

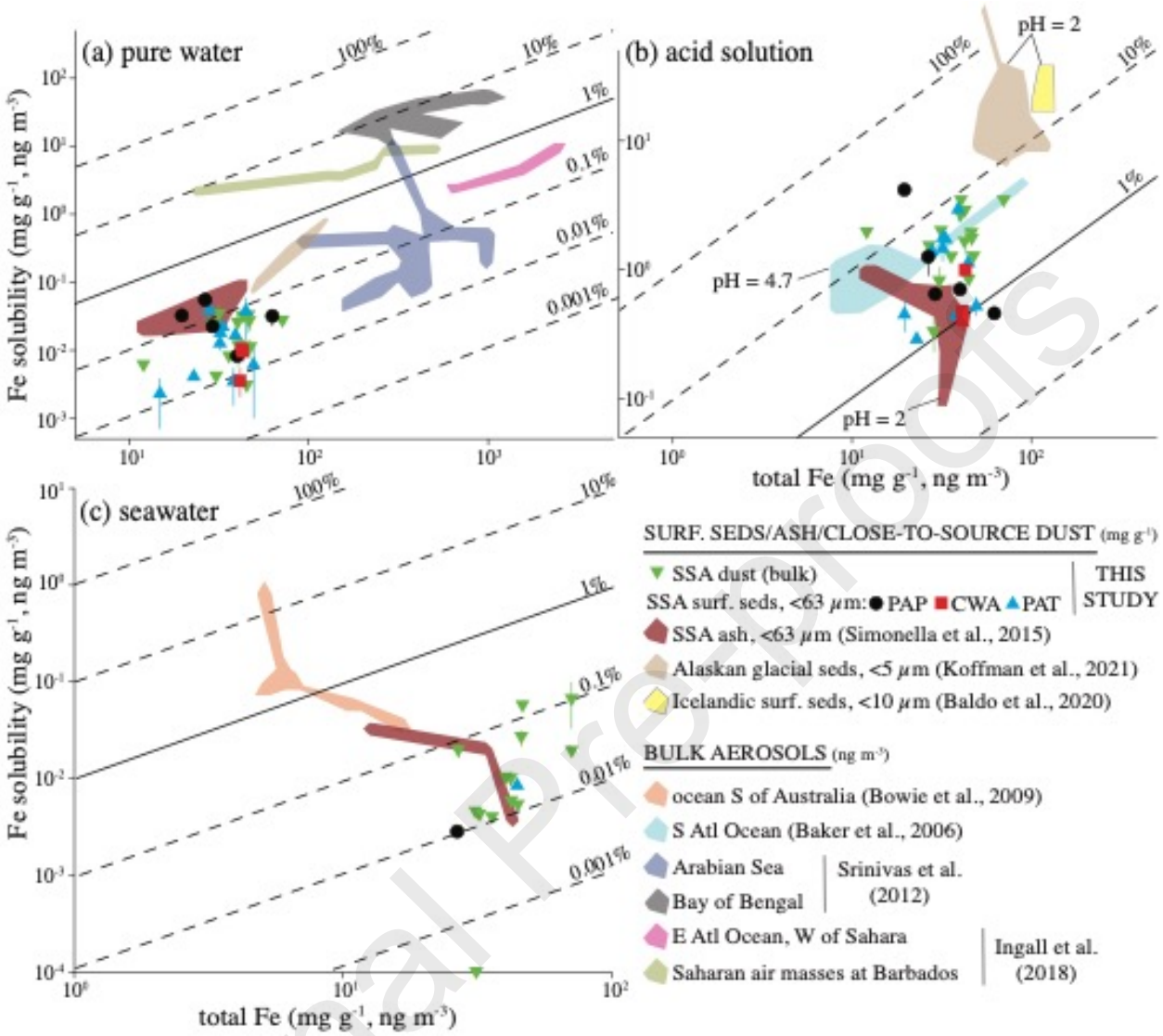

Figure 2. Iron solubility vs. total Fe for dust (bulk) and dust-emitting surface sediments (<63 μm) of southern South America (SSA), based on leaching experiments with (a) pure (i.e., Milli-Q) water for 20 min, (b) pH = 2 nitric acid solution for 2 h, and (c) seawater. Horizontal (a-c) and vertical (a-b) error bars for this study's measurements are 1σ based on three determinations and are smaller than the symbols if not visible. PAP: Puna-Altiplano Plateau, CWA: Central Western Argentina, PAT: Patagonia, Atl: Atlantic.

Table 2. Iron solubility velocity index (T_{Fe_sol}, minutes) of dust and dust-emitting surface sediments.

sample name	Milli-Q extraction			1% HNO_3 extraction			seawater extraction	
	<63 μm	<11 μm	bulk	<63 μm	<11 μm	bulk	<63 μm	bulk
Puna-Altiplano Plateau								
SAB1	7.2	7.6	nd	26.3	33.5	nd	nd	nd
SAB2	1.3	9.8	nd	41.2	42.2	nd	56.5	nd
SAB3	8.8	13.5	nd	28.7	44.7	nd	nd	nd

SAB4	nd	5.5	nd	nd	33.8	nd	nd	nd
SPU5	2.3	5.7	nd	40.2	26.7	nd	nd	nd
S27	nd	nd	nd	nd	n.d.	nd	nd	19.9
SPU6	4.5	6.0	nd	29.3	49.8	nd	nd	nd
Central Western Argentina								
SCOA8	3.8	9.0	nd	54.3	58.7	nd	nd	nd
SCOA9	2.3	2.7	nd	45.0	48.3	nd	nd	nd
SCOA10	nd	9.7	nd	nd	37.5	nd	nd	nd
SCOA11	2.3	9.2	nd	47.8	34.0	nd	nd	nd
Pampean plains (east of South American Arid Diagonal)								
MJ166	nd	nd	nd	nd	nd	nd	nd	37.0
MJ205	nd	nd	nd	nd	nd	nd	nd	10.9
Temperley	nd	nd	7.6	nd	nd	39.5	nd	nd
Patagonia								
SPA12	5.3	8.3	nd	41.7	42.7	nd	nd	nd
BB8	nd	nd	nd	nd	nd	nd	nd	44.3
SPA13	6.7	10.0	nd	36.7	28.8	nd	nd	nd
SPA14	2.5	7.5	nd	47.0	48.0	nd	46.1	nd
TW7	nd	nd	nd	nd	nd	nd	nd	51.6
TW10	nd	nd	6.5	nd	nd	36.1	nd	38.0
TW94	nd	nd	nd	nd	nd	nd	nd	55.6
SPA15	7.2	10.2	nd	55.2	47.2	nd	nd	nd
SPA16	6.0	4.3	nd	45.0	51.8	nd	nd	nd
SPA17	7.8	8.0	nd	38.7	28.7	nd	nd	nd
SPA18	5.5	11.7	nd	26.7	39.3	nd	nd	nd
SJ16-CP	nd	nd	8.1	nd	nd	37.6	nd	41.8
SPA19	2.3	10.0	nd	30.7	36.0	nd	nd	nd
SPA20	5.8	9.7	nd	42.3	43.0	nd	nd	nd
SPA21	7.8	nd	nd	38.2	nd	nd	nd	nd
RG13	nd	nd	9.2	nd	nd	41.4	nd	55.4
RG18	nd	nd	nd	nd	nd	nd	nd	26.1
RG22	nd	nd	7.9	nd	nd	40.4	nd	38.3
RG82	nd	nd	nd	nd	nd	nd	nd	23.2
RG89-BSNE	nd	nd	nd	nd	nd	nd	nd	2.4
RG89-CP	nd	nd	nd	nd	nd	nd	nd	25.7
RG104	nd	nd	nd	nd	nd	nd	nd	3.0

nd: not determined

While Fe_{MQ} of Patagonian dust-emitting surface sediments is broadly equally distributed between the <63-μm and <11-μm fractions, most samples from CWA and all samples from PAP show higher Fe solubilities in the <63-μm and <11-μm fractions, respectively (Figure 3a). Instead, for 1% nitric acid extraction the vast majority of surface sediment samples show higher Fe_{AC} for the <11-μm fraction (Figure 3b).

3.3 Mineralogy and Chemical Index of Alteration

Taken as a whole, the mineralogical composition of surface sediments (<63 μm) across the SAAD consists of clays (except chlorite and pyrophyllite, 31 ± 11%, 1σ), plagioclase (26 ± 12%), quartz (20 ± 10%), calcite (8 ± 10%), K-feldspar (6 ± 5%) and other mineral phases (pyrophyllite, gypsum, amphibole and hematite, 5 ± 5%) (Table S4). The mineralogy of the <11-μm fraction of surface sediments is similar, with slightly higher mean fractions of clays (35%) and calcite (11%). Compared to the coarsest fraction, the finest fraction (<5 μm) has higher mean amounts of clays (40%), calcite (13%) and halite (12%). Of all minerals, calcite and halite show the greatest variability across surface sediments. The highest contributions of calcite are found in alluvial fans of the PAP and topsoils and ephemeral lakes of Patagonia, while halite dominates in alluvial fans and salar edges of PAP and ephemeral lakes of Patagonia. Two dust samples from Patagonia and one dust sample collected in the city of Buenos Aires and derived from PAP more than 1,500 km downwind (Gaiero et al., 2013) show a mean mineral composition that is indistinguishable within uncertainty to that of the <63-μm fraction of surface sediments, with a dominance of quartz (32 ± 9%), clays (24 ± 5%), plagioclase (22 ± 9%) and K-feldspar (17 ± 19%). However, when the bulk mineralogical composition of the two close-to-source Patagonian dust samples (i.e., TW14 and RG29) are compared against the <63-μm fraction of their

respective closest sampled surface sediments (i.e., SPA14/SPA15 and SPA21, respectively), there is a clear depletion in total clays, and an enrichment in quartz and K-feldspar (Table S4).

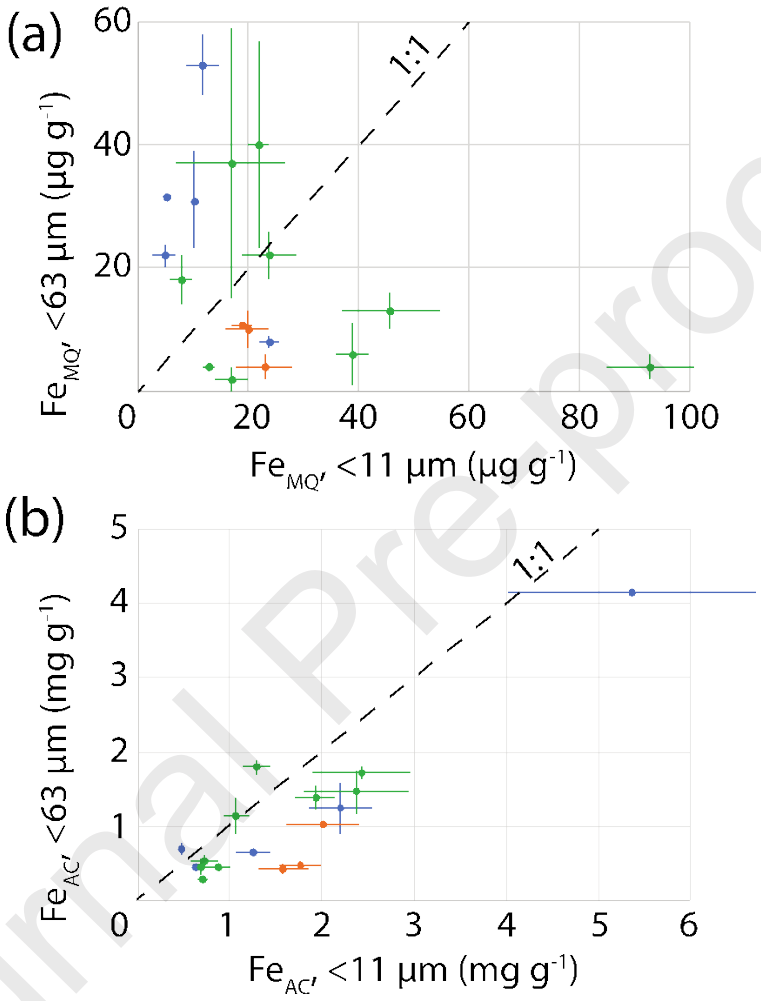

Figure 3. Iron solubility of southern South American dust-emitting surface sediments for the <63 µm and <11 µm optical diameter fractions, in (a) Milli-Q water (Fe_{MQ}) and (b) 1% nitric acid (Fe_{AC}). Blue, orange and green points correspond to central-western Argentina, Puna-Altiplano Plateau and Patagonia samples, respectively. Solubilities are expressed as micro- or milli-grams of Fe per gram of total sample. Error bars correspond to 1σ. Dash lines indicate equal proportions.

The strongest correlation between median grain size-normalized FFS of surface sediments (<63 µm) and any single mineralogical parameter is with total clay content (Figure 4), with a slightly

higher positive correlation for acid (non-parametric Spearman test of correlation: r = 0.74, p = 0.001, Figure 4b) than for water (r = 0.69, p = 0.004, Figure 4a) leaching experiments.

The CIA of surface sediments (<63 μm) across the SAAD ranges between 42-67, with a mean of 58 ± 7 (1σ), with no regional grouping (Table 2).

3.4 Iron speciation

The solid iron oxidation state of dust-emitting surface sediments across the SAAD is dominated by paramagnetic Fe^{3+} over paramagnetic Fe^{2+} (Fe^{2+}: 39 ± 15%, 1σ, Table 2). Two samples from ephemeral lakes in Patagonia contain particularly high Fe^{2+} vs. Fe^{3+} (SPA17 and SPA21, >50%), while salar edge and playa lake samples from PAP and Patagonia show particularly low Fe^{2+} vs. Fe^{3+} (SAB3 and SPA14, <20%). Paramagnetic interactions dominate in Fe: 50 ± 15% of all contributions (Fe^{3+} and Fe^{2+}) are due to Fe^{3+} in paramagnetic environments (Table S5). In fact, median grain size-normalized FFS_{AC} (<63 μm) correlates with the proportion of paramagnetic Fe^{3+} in Fe_{TOT} (r = 0.67, p = 0.023, Figure 5), and does not correlate with the proportion of any other magnetic phase in Fe_{TOT}. Another, smaller contribution to Fe^{3+} derives from hematite, and to a lesser extent magnetite, the former of which was also identified by XRD. This contribution of hematite and magnetite is observed for surface sediments in PAP and CWA, with very few to no contribution in Patagonian samples.

4 Discussion

4.1 Low fertilization potential of present-day South American dust

Fe_{MQ} is intended to mimic Fe release during interactions with non-acidic atmospheric water during transport and is thus appropriate to evaluate the source-inherited Fe solubility of dust (Chomchoei et al., 2005; Simonella et al., 2014). There are differences however between ultra-

pure water and naturally occurring, non-acidic rainwater, the two most important of which in terms of Fe solubility are the presence of natural ligands and buffering capacity (e.g., Paris and Desboeufs, 2013; Shelley et al., 2018). Our flow-through leaching experiments show FFS_{MQ} for SSA close-to-source bulk dust and dust-emitting, <63-µm surface sediments (i.e., 0.054%) that lie in the lower end of a global range (i.e., 0.001-90%) that includes dust of varying compositions, including mixing with other types of aerosols, physical characteristics, distance to sources, and leaching methods (Desboeufs et al., 1999, 2001; Jickells and Spokes, 2001; Bonnet and Guieu, 2004; Hand et al., 2004; Mahowald et al., 2005; Sholkovitz et al., 2012; Baker et al., 2006, 2013; Simonella et al., 2015; Koffman et al., 2021).

Compared to Fe_{MQ} of other source or close-to-source wind-borne materials globally, SSA dust and sediments show similar values to <20-µm loess samples that constitute Saharan dust precursors (<0.1%, Desboeufs et al., 1999, 2001), but significantly lower than Alaskan <5-µm sediments and loess of glacial origin (Koffman et al., 2021) and <63-µm fresh ashfall deposits derived from southern Andean volcano eruptions of varying compositions (Simonella et al., 2015, Figure 2a). While present-day dust-emitting surface sediments in SSA are for the most part non-glacial in origin, the comparison against glacial sediments is particularly relevant because it is believed that dust emitted during the last glacial period in SSA was derived mostly from glaciofluvial flour exposed on Patagonian outwash plains (Sudgen et al., 2009). The difference in Fe_{MQ} between SSA surface sediments/dust and Alaskan glacial-derived sediments is even higher than depicted in Figure 2a considering that Fe_{MQ} release after 20 mL of total flow-through ultra-pure water volume was negligible in similar SSA samples (Simonella et al., 2014), while Koffman et al. (2021) used a total flow-through volume of 1 L and similar Alaskan sediments showed a five-fold increase in FFS_{MQ} when total leaching volume was raised from 750 mL to 5 L

(Schroth et al., 2009). The control of grain size on SSA Fe_{MQ} is weak (Figure 3a) and thus differences in sample grain size cannot account for SSA-Alaskan differences in Fe_{MQ}. Besides, the <5-µm fraction of Alaskan sediments was obtained by wet sieving (Koffman et al., 2021), which could have extracted soluble Fe prior to the leaching experiments, further enlarging the difference between Fe_{MQ} of SSA and Alaska samples.

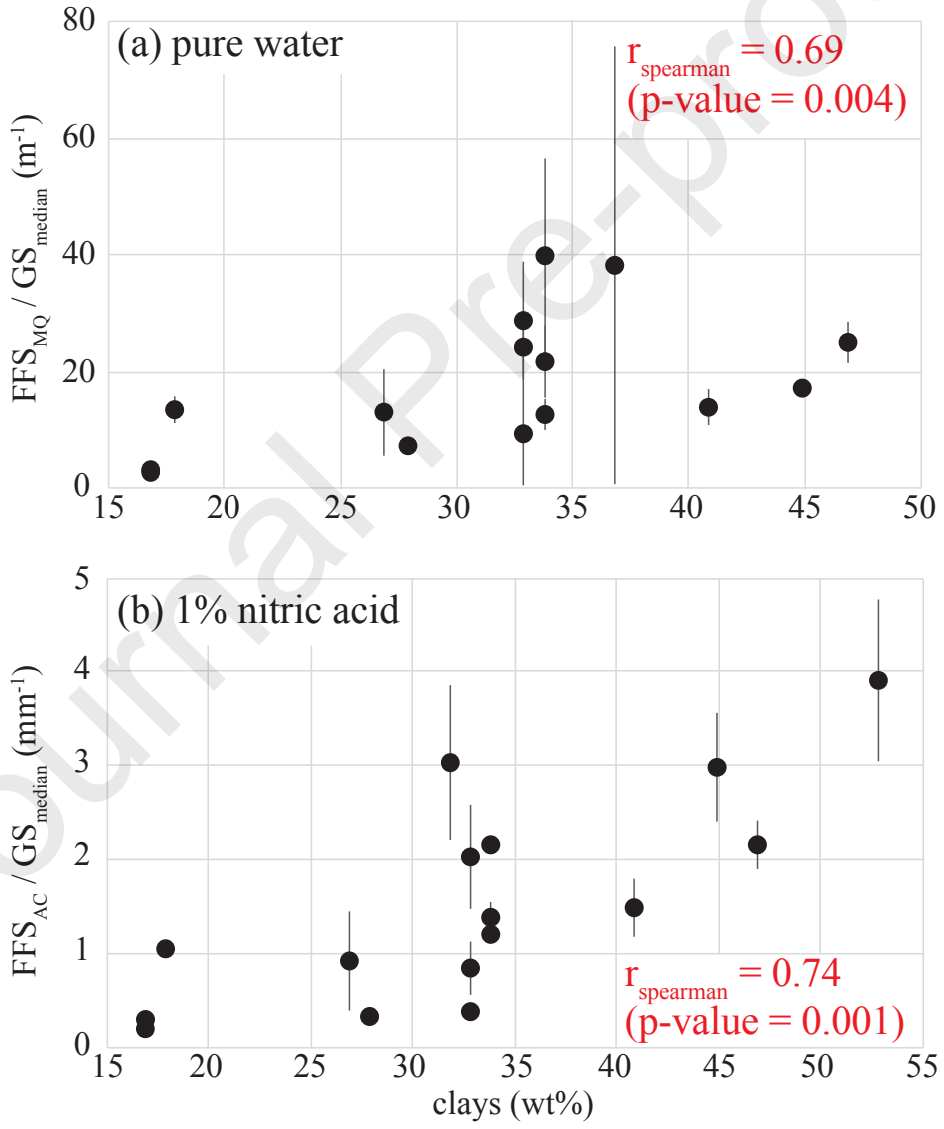

Figure 4. Fractional Fe solubility (FFS) of southern South American dust-emitting surface sediments in (a) Milli-Q water (FFS_{MQ}) and (b) 1% nitric acid (FFS_{AC}), for the <63-µm optical diameter fraction, normalized to median grain size (GS), as a function of the percentage of clays present in the samples. Outliers were defined as data points that exceed 2σ of the mean of either one of the two axis (or both), and were not considered for calculation of the non-parametric Spearman coefficient of correlation ($r_{spearman}$). Three (two) outliers were identified for the pure water (1% nitric acid) dataset. Error bars in the y axis are 1σ (if not visible, bars are smaller than the data points).

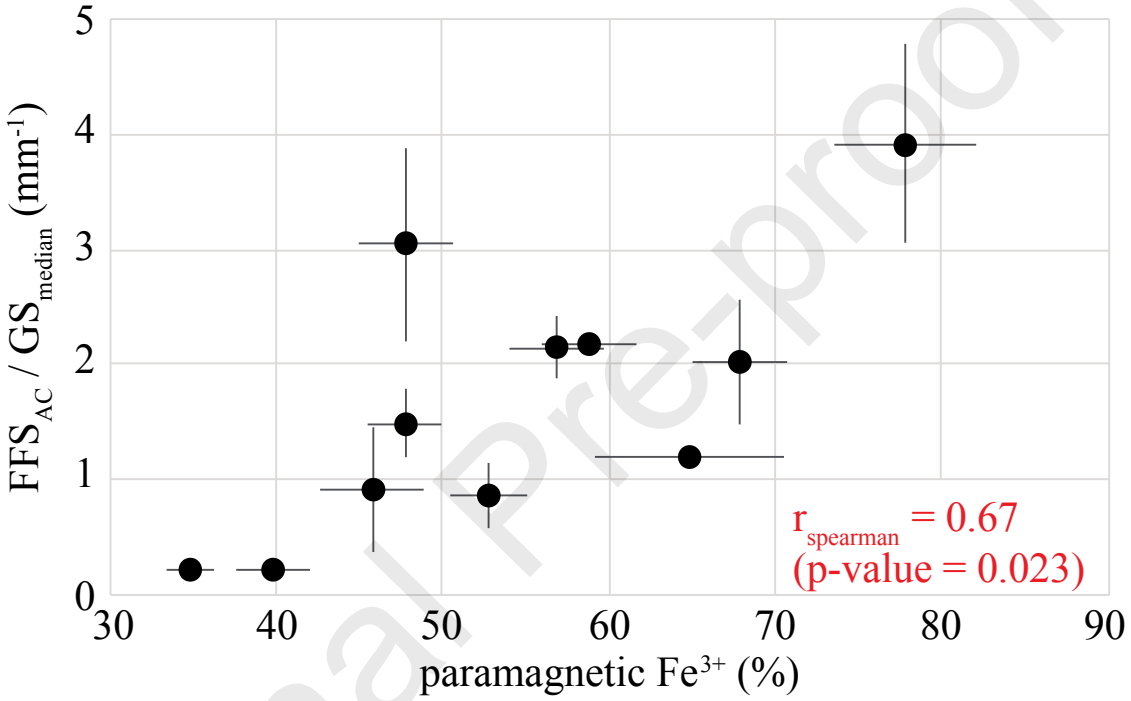

Figure 5. Fractional Fe solubility (FFS) of southern South American dust-emitting surface sediments in 1% nitric acid (FFS_{AC}), for the <63 µm optical diameter fraction, normalized to median grain size (GS), as a function of the fraction of Fe present as paramagnetic Fe^{3+}. Outliers were defined as data points that exceed 2σ of the mean of either one of the two axis (or both), and were not considered for calculation of the non-parametric Spearman coefficient of correlation ($r_{spearman}$). Two outliers (> 2σ in either axis) were discarded. Error bars are 1σ (if not visible, bars are smaller than the data points).

While our Fe_{MQ} measurements of SSA close-to-source dust and dust source sediments reflect processes that are very different from those reflected by similar measurements in open-ocean aerosols, comparing these two sets of measurements can shed light on the role of atmospheric

processing and anthropogenic influences. Figure 2a shows the comparison of our measurements against a global compilation consisting mostly of shipborne bulk aerosol samples. While Fe_{TOT} and Fe solubility cannot be directly compared between these two data sets, given that Fe in SSA samples is quantified against total sediment/dust mass while in open-ocean aerosols it is quantified against total air volume, both data sets can be compared in terms of FFS. Samples collected on the eastern Atlantic Ocean west of the Sahara Desert represent close-to-source Saharan dust that has not yet been intensely processed in the atmosphere. These samples (Ingall et al., 2018) show FFS_{MQ} higher than SSA fresh ash (Simonella et al., 2015) dust and surface sediments, which probably reflects the influence of African oil combustion emissions (Rodríguez et al., 2021) and a lack of such an influence in Patagonia. This influence of anthropogenic pollutants on dust soluble Fe can be appreciated when comparing aerosols sampled at the Bay of Bengal and Arabian Sea (Srinivas et al., 2012). While dust in both regions has traveled similar distances from their respective sources, Fe_{MQ} in dust from the Bay of Bengal is two orders of magnitude higher, due to a stronger impact of fossil-fuel combustion and biomass burning (Srinivas et al., 2012).

After considerable atmospheric transport has taken place, Saharan air masses in Barbados display an order of magnitude or higher FFS_{MQ} (Ingall et al., 2018, Figure 2a). This is consistent with a similar finding where FFS_{SW} was up from 0.7% close to Saharan sources in Tenerife to 4.7% across the Atlantic Ocean in Miami (Rodríguez et al., 2021). This is despite a similar influence of oil combustion on FFS_{SW} in the Tenerife (10%) and Miami (16%) sampling sites, which suggests a solubility enhancement due to atmospheric processing (Rodríguez et al., 2021). Such atmospheric processes include iron reduction due to inorganic acids, organic species and photochemical reactions (Baker and Croot, 2010; Breitbarth et al., 2010; Bligh and Waite, 2011;

Raiswell and Canfield, 2012; Paris and Desboeufs, 2013), reduction in pH in the vicinity of dust particles due to absorption of acid gases (Hegg et al., 2002; Straub et al., 2007), evaporation of water droplets (Zhu et al., 1992; Meskhidze et al., 2003), repeated cycles of humidity and evaporation (Pruppacher and Jaenicke, 1995; Uno et al., 2009), or absence of buffering species such as carbonates (Ito and Feng, 2010), or progressive fining of dust due to selective deposition of coarser particles and associated rises in reactivity due to higher surface-to-volume ratios (Baker and Jickells, 2006; Cwiertny et al., 2008).

In SSA close-to-source dust and dust-emitting surface sediments, FFS_{AC} (Figure 2b) is two orders of magnitude higher than FFS_{MQ} (Figure 2a), so that labile Fe is dominated by the acid-soluble, water-insoluble fraction. The fractional solubility of labile Fe (FFS_{MQ+AC}) in SSA fresh ashfall deposits is somewhat lower than that of SSA surface sediments/ash (Figure 2b), which is opposite to FFS_{MQ} (Figure 2a). Compared to dust-emitting surface sediments in Alaska (Koffman et al., 2021) and Iceland (Baldo et al., 2020), FFS_{MQ+AC} in SSA surface sediments is 5-8 times lower (Figure 2b). While part of this difference in FFS_{MQ+AC} may be due to differences in grain size, FFS_{MQ+AC} in SSA surface sediments is only 20% higher in the <11-µm than in the <63-µm fraction (Figure 3b). Another relevant data set against which to compare our results are bulk aerosols from the southern Atlantic Ocean (Figure 2b) which include samples collected directly downwind of Patagonia in October 2001 (Baker et al., 2006). FFS of these samples under pH = 4.7 extraction solutions is similar to the upper end of FFS_{MQ+AC} in Patagonian sediment and dust samples. Considering (1) that similar values of FFS were obtained under much less acidic conditions in aerosols sampled 600-700 km from Patagonian dust sources, and (2) the relative pristine conditions of the atmosphere offshore Patagonia may indicate that some degree of atmospheric processing not associated to the presence of atmospheric pollutants indeed takes

place in this region, possibly associated to natural SO_2 emissions. While it cannot be ascertained that dust was an important contributor to these open-ocean aerosol samples, at least one of these samples had a coloration typical of dust, and back trajectory simulations point to continental Patagonia as a likely source (Baker et al., 2006). Also, a climatology for October displays intermediate dust activity in central and northern Patagonia (Cosentino et al., 2021).

Soluble Fe released in seawater by SSA dust samples was very similar to that in ultra-pure water as a fraction of Fe_{TOT} (Figure 2c). It is also comparable to Fe released from SSA fresh ashfall deposits (Simonella et al., 2015), but two orders of magnitude lower than open-ocean bulk aerosols sampled south of Australia, with a significant contribution from dust (Bowie et al., 2009). Low values of Fe_{SW} in SSA dust indicate a reduced pool of potentially bioavailable Fe through dry deposition of dust on the oceans.

Low FFS_{MQ}, FFS_{AC} and FFS_{SW} of SSA dust and dust-emitting surface sediments when compared to global compilations of similar measurements all point to a low fertilization potential of present-day SSA dust. This is consistent with a lack of response of satellite chlorophyll-a in continental shelf and open-ocean waters to deposition of Patagonian dust during non-limiting light conditions in the austral summer (Johnson et al., 2011; Cosentino et al., 2020a).

4.2 Controls on labile iron in South American dust and dust-emitting surface sediments

Given the many physical and chemical parameters that may be jointly controlling labile Fe in South American dust-emitting surface sediments, we performed principal component (PC) analysis (PCA) to explore potentially complex relationships between different parameters. The two main PCs jointly explain 45% of the total sample variance (Figure 6). Fe_{AC} shows a high positive correlation with total clay content, consistent with bivariate analysis (Figure 4b). A high

negative correlation of Fe_{AC} with magnetic Fe^{3+} is also found, as well as a not-as-strong negative correlation with median grain size (Figure 6). These three correlations are consistent with clays being the main mineral phases contributing Fe_{AC}, given the paramagnetic nature of Fe in clays, and the rise in total clay content for finer-grained fractions (Table S4). Moreover, phyllosilicates such as pyrophyllite have been identified by XRD in these samples. While we have not performed chemical analyses that allow discrimination of clays in our samples, previous studies have shown a dominance of illite and chlorite in dust-emitting surface sediment samples (<2 μm) of the PAP in the northern sector of the SAAD, a dominance of smectite in equivalent samples from northern Patagonia in the central SAAD, and a mixture from both clay groups in the southern CWA (Gaiero et al., 2004; Hepper et al., 2006; Romero et al., 2021). The predominant role of clays in delivering acid-soluble Fe is supported by single-mineral leaching experiments at conditions similar to that of this study (pH = 2), which also show low contributions from Fe (hydr-)oxides (e.g., Journet et al., 2008; Marcotte et al., 2020).

Considering that ferrihydrite is commonly found in the surface of clays (Shi et al., 2011a), we cannot rule out the possibility that this phase is contributing to the paramagnetic signal of our dust-emitting surface sediment samples, given that (1) the hyperfine parameters of ferrihydrite are similar to those of phyllosilicates (McCammon, 1995), and (2) the absence of ferrihydrite in the XRD patterns can be explained by the lack of well-defined and intense diffraction peaks (e.g., Eggleton, 1987).

While the observed bivariate correlation between Fe_{AC} and paramagnetic Fe^{3+} (Figure 5) is much stronger than that of Fe_{AC} and paramagnetic Fe^{2+} (not shown), PCA shows only a slightly stronger clustering of Fe_{AC} with paramagnetic Fe^{3+} than with paramagnetic Fe^{2+}, which may be interpreted as a weaker influence of Fe oxidation state on Fe solubility compared to Fe bonding

environment. This is in part supported by leaching experiments showing orders of magnitude lower Fe solubility in Fe^{3+}-dominated (hydr-)oxides compared to Fe^{3+}-dominated sulfates (Schroth et al., 2009). It is also in part supported by in situ measurements showing similar ocean dissolved Fe for sediment sources derived from similar parent rocks (i.e., similar Fe-bearing mineral phases), but with a wide range of Fe^{2+}:Fe^{3+} ratios (van Genuchten et al., 2021).

The PCA-derived negative correlation of Fe_{AC} with median grain size (Figure 6) is consistent with the fact that bivariate correlations of Fe_{AC} are generally improved when normalized with median grain size (Figures 4b-5). Several previous studies have found equivalent relationships between dust grain size and Fe release under weak acid leaches (e.g., Baker and Jickells, 2006; Shi et al., 2011b). Instead, our PCA results show no control of grain size on Fe_{MQ} in SSA dust-emitting surface sediments (Figure 6), in line with a lack of a trend of Fe_{MQ} in a highly size-resolved set of Atlantic aerosol samples (Buck et al., 2010). This difference in grain size dependence between Fe_{MQ} and Fe_{AC} may reflect the fact that (1) weakly bound Fe in clays' mineral lattices is only extracted under at least weakly acidic solutions (Poulton and Canfield, 2005; Journet et al., 2008; Ryan et al., 2008), and (2) clays are enriched in the finer fractions of SSA dust-emitting surface sediments (Table S4). Faster Fe_{MQ} release compared to Fe_{AC} (5-8x, Table 1) arguably reflects this difference in mineral phases contributing to the labile Fe pool, with only non-structurally bound Fe adsorbed to the surface of silicate phases (clays or otherwise) released under non-acidic solutions, and weakly bound Fe in silicate phases leached under weakly acidic conditions.

The main PCA-derived positive correlation of Fe_{MQ} is against the concentration of secondary mineral gypsum, and to a lesser degree halite and calcite (Figure 6). Several samples across the SAAD with particularly high concentrations of these minerals are sourced from ephemeral lake

and playa environments (e.g., SAB3, SPA13, SPA17, SPA19). These positive correlations may be indicative of the association of gypsum and calcite with Fe sulfates and carbonates in these closed-basin, evaporative environments (Shi et al., 2011c). The positive correlations between Fe_{MQ} and both LOI and LOI_{105^oC} are consistent with this interpretation, given the low gypsum-anhydrite equilibrium temperature under surface pressure (Zanbak and Arthur, 1986).

4.3 Implications for biogeochemical impacts of South American dust during glacial times

Active glacial processes in Patagonia are restricted to the upper valleys of the Andes, with reduced delivery of glacially derived sediments to the eastern outwash plains due to the presence of proglacial lakes (Gaiero et al., 2003). Thus, present-day dust sources in Patagonia, as sampled in this study, are predominantly non-glaciogenic (Table S1) and located within a narrow band <150 km from the eastern coast (Figure 1). Shoenfelt et al. (2017) found that similar non-glaciogenic Holocene lake sediment samples, likely derived from chemically weathered rocks, did not boost diatom productivity in culture experiments, which may explain why present-day dust emissions from eastern Patagonia do not enhance oceanic primary producers' biomass (Johnson et al., 2011; Cosentino et al., 2020a). Instead, glaciogenic samples derived from (1) recently deposited (<150 years), and (2) Last Glacial Maximum (LGM) moraines, all having experienced low chemical weathering, did raise model diatom growth rates (Shoenfelt et al., 2017). While dust sources are currently predominantly non-glaciogenic, there is evidence to suggest that during glacial periods, Patagonian dust delivered to the South Atlantic was glaciogenic and highly bioavailable (Shoenfelt et al., 2018).

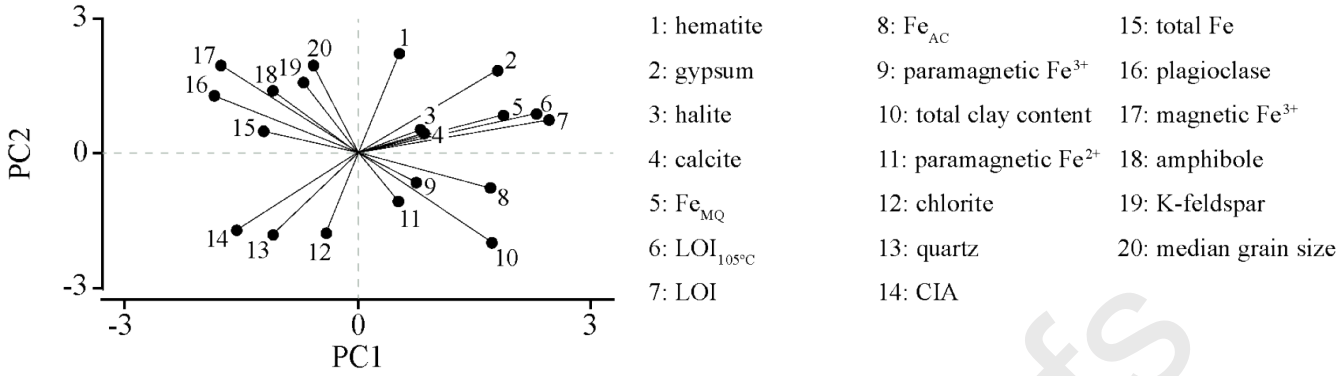

Figure 6. Principal component analysis for surface sediment samples (<63 μm). The first and second principal components are shown, which explain 25.8% and 19.1% of the data set variance, respectively.

The strong negative correlation between Fe_{MQ} and CIA for present-day dust-emitting surface sediment samples (<63 μm) across the SAAD (Figure 6) seems to suggest that higher degrees of chemical weathering result in low values of source-inherited Fe solubility of SSA dust sources (Shi et al., 2011c; Shoenfelt et al., 2019). Given the shift to higher precipitation after the LGM in eastern Patagonia (Berman et al., 2016), CIA values of present-day dust-emitting surface sediments in the region are probably a proxy for time-integrated chemical weathering since the beginning of the last deglaciation. Calculated CIA values for our surface sediment samples (58 ± 7, 1σ) are higher than mean upper continental crust (48, Taylor and McLennan, 1985), which may be considered representative of fresh rock, similar to LGM (67 ± 8) and lower than current interglacial (76 ± 9) dust in Eastern Antarctic ice core EPICA Dome C (Marino et al., 2008). Thus, compared to other dust sources in the Southern Hemisphere, SSA dust sources seem to have experienced reduced, albeit non-negligible chemical weathering since the last deglaciation. Nonetheless, this low degree of chemical weathering may have been sufficient to deplete sediments of highly labile, water-soluble iron.

The lack of correlation between Fe_{MQ} and grain size (Figure 6) may have broader implications for the input of atmospheric soluble Fe to the glacial southern oceans. Dust grain size is sub-estimated in global Earth system models, with simulated >5-μm fractions in the atmosphere usually under-predicted against measurements (Adebiyi and Kok, 2020). In SSA, the GSD of dust-emitting surface sediments (<63 μm) and dust (bulk) collected close to the sources display medians that vary widely (~7-67 μm) and average at ~27 μm (Table 2). This is considerably coarser than the maximum dust grain size simulated in the past using regional models such as GOES-Chem (i.e., 12 μm) to look at the fertilization effect of Patagonian dust on the South Atlantic Ocean (Johnson et al., 2010, 2011). While the present-day fertilization potential of SSA dust is low based on evidence presented in this study, we argue that during glacial periods this potential has probably been higher, and that the contribution of coarse dust to this potential may be underestimated. This is because (1) dust events in SSA have been identified where dust deposited after >1000 km of transport peaks at 14 μm with >30% by volume represented by the >20-μm fraction (Gaiero et al., 2013), (2) high-nutrient, low-chlorophyll regions most susceptible to dust fertilization are located downwind of Patagonia at relatively short distances from the sources, starting at ~600 km from the eastern Patagonian coast, and (3) the independence of Fe_{MQ} with grain size imply that source-inherited Fe solubility of coarse and fine dust particles is similar. We thus stress the importance of correctly representing dust grain size in models that try to gauge the effect of desert and glaciogenic dust as ocean fertilizers (e.g., Yamamoto et al., 2019), particularly during glacial times when a drier climate may have implied less wet-phase atmospheric processing and less continental chemical weathering, and thus soluble Fe inputs to the oceans may have arguably been controlled more strongly by source-inherited Fe solubility.

5 Conclusions

When compared to global compilations of similar data, low FFS_{MQ}, FFS_{AC} and FFS_{SW} of SSA dust sources and close-to-source dust all point to a low fertilization potential of present-day SSA dust. This may explain why studies using satellite chlorophyll-a in HNLC open ocean waters do not show apparent responses to deposition of SSA dust during non-limiting light conditions in the austral summer. Water-soluble Fe solubility is correlated with gypsum, and to a lesser extent, calcite and halite abundances, which may reflect the association of these minerals with water-soluble Fe sulfates and carbonates in evaporitic environments of SSA. Instead, labile Fe (Fe_{MQ} + Fe_{AC}) is correlated with total clay content, grain size and paramagnetic Fe, with oxidation state of Fe playing a smaller role. This is consistent with clays being the main mineral phases carrying labile Fe in our samples.

While present-day dust from SSA has low fertilization potential, multiple lines of evidence suggest a stronger ocean biogeochemical influence during glacial times. First, present-day active dust sources, as sampled in this study, are predominantly non-glaciogenic, while the contribution of glaciogenic dust sources to total dust emissions in SSA during glacials must have been higher. Modern and LGM glaciogenic sediments in Patagonia have been shown to enhance primary productivity in culture experiments. Second, if a similar independence of Fe_{MQ} in present-day SSA dust sources and close-to-source dust on grain size (as found in this study) holds for glaciogenic sources in glacial times, then the role of coarse dust as a supplier of bioavailable Fe to the glacial southern oceans may be underestimated. This is because the coarse fraction of dust dominates by mass, and HNLC regions downwind of SSA are close enough to the sources that this coarse fraction may reach them. Last, Fe speciation of marine sediments during glacial times

in the South Atlantic Ocean suggests that indeed fluxes of bioavailable Fe were higher than during interglacials.

Acknowledgments

This work was financed by project ANPYCT-PICT-2017-2705 to DMG. NJC acknowledges support from project ANID-FONDECYT-POSTDOCTORADO2020-3200085. MLM acknowledges support from the Argentine Ministry of Science (project ANPYCT-PICT-2018-01536), the UNLP School of Exact Sciences (project 11X/847) and CONICET (projects PUE 066 and PIP 0987). PLC acknowledges that his aerosol research is supported in part by a research grant from Science Foundation Ireland (SFI) under grant number 13/RC/2092 and co-funded under the European Regional Development Fund and by iCRAG industry partners. We appreciate comments by the Associate Editor and two anonymous reviewers that greatly improved this manuscript. Reanalysis data from ERA5 may be extracted at https://cds.climate.copernicus.eu. New data generated in this study can be found in Tables 1-2, as well as in the Supplementary Material. This data will be deposited in the EarthChem online repository upon acceptance of this manuscript for publication.

Appendix A. Supplementary Material

The main supplementary material file contains figures showing dust collectors used in this study, as well as their deployment on the field, and examples of surfaces where dust-emitting surface sediments were sampled. Also included are figures showing examples of XRD and Mössbauer spectra fitting. Tabulated data include information of sampled sites, results from the iron leaching experiments, grain size, grain size-resolved mineralogy based on powder XRD analysis and Mössbauer-derived magnetic iron phases.

References

Adebiyi A. A. and Kok J. F. (2020) Climate models miss most of the coarse dust in the atmosphere. *Sci. Adv.* **6**(15), eaaz9507.

Baker A. R. and Jickells T. D. (2006) Mineral particle size as a control on aerosol iron solubility. *Geophys. Res. Lett.* **33**(17).

Baker A. R., Jickells T. D., Witt M. and Linge K. L. (2006) Trends in the solubility of iron, aluminium, manganese and phosphorous in aerosol collected over the Atlantic Ocean. *Mar. Chem.* **98**(1), 43-58.

Baker A. R. and Croot P. L. (2010) Atmospheric and marine controls on aerosol iron solubility in seawater. *Mar. Chem.* **120**(1-4), 4-13.

Baker A. R., Adams C., Bell T. G., Jickells T. D. and Ganzeveld L. (2013) Estimation of atmospheric nutrient inputs to the Atlantic Ocean from 50° N to 50° S based on large-scale field sampling: Iron and other dust-associated elements. *Global Biogeochem. Cycles*, **27**(3), 755-767.

Baldo C., Formenti P., Nowak S., Chevaillier S., Cazaunau M., Pangui E., Di Biagio C., Doussin J.-F., Ignatyev K., Dagsson-Waldhauserova P., Arnalds O., MacKenzie A. R. and Shi Z. (2020) Distinct chemical and mineralogical composition of Icelandic dust compared to northern African and Asian dust. *Atmos. Chem. Phys.* **20**(21), 13521-13539.

Berman A. L., Silvestri G. E. and Tonello M. S. (2016) Differences between Last Glacial Maximum and present-day temperature and precipitation in southern South America. *Quat. Sci. Rev.* **150**, 221-233.

Bligh M. W. and Waite T. D. (2011) Formation, reactivity, and aging of ferric oxide particles formed from Fe (II) and Fe (III) sources: Implications for iron bioavailability in the marine environment. *Geochim. Cosmochim. Acta* **75**(24), 7741-7758.

Bonnet S. and Guieu C. (2004) Dissolution of atmospheric iron in seawater. *Geophys. Res. Lett.* **31**(3).

Boski T., Pessoa J., Pedro P., Thorez J., Dias J. M. A. and Hall I. R. (1998) Factors governing abundance of hydrolyzable amino acids in the sediments from the N.W. European Continental Margin (47-50ºN). *Prog. Oceanogr.* **42**(1-4), 145–164.

Bowie A. R., Lannuzel D., Remenyi T. A., Wagener T., Lam P. J., Boyd P. W., Guieu C., Townsend A. T. and Trull T. W. (2009) Biogeochemical iron budgets of the Southern Ocean soth of Australia: Decoupling of iron and nutrient cycles in the subantarctic zone by the summertime supply. *Global Biogeochem. Cycles* **23**(4).

Breitbarth E., Achterberg E. P., Ardelan M. V., Baker A. R., Bucciarelli E., Chever F., Croot P. L., Duggen S., Gledhill M., Hassellöv M., Hassler C., Hoffmann L. J, Hunter K. A., Hutchins D. A., Ingri J., Jickells T., Lohan M. C., Nielsdóttir, M. C., Sarthou G., Schoemann V., Trapp J. M.,

Turner D. R. and Ye Y. (2010) Iron biogeochemistry across marine systems–progress from the past decade. *Biogeosciences* **7**(3), 1075-1097.

Browning T. J., Bouman H. A., Henderson G. M., Mather T. A., Pyle D. M., Schlosser C., Woodward E. M. S. and Moore C. M. (2014) Strong responses of Southern Ocean phytoplankton communities to volcanic ash. *Geophys. Res. Lett.* **41**, 2851–2857.

Browning T. J., Achterberg E. P., Engel A. and Mawji E. (2021) Manganese co-limitation of phytoplankton growth and major nutrient drawdown in the Southern Ocean. *Nat. Commun.* **12**, 884.

Buck C. S., Landing W. M. and Resing J. A. (2010) Particle size and aerosol iron solubility: A high-resolution analysis of Atlantic aerosols. *Mar. Chem.* **120**(1-4), 14–24.

Cassar N., Bender M. L., Barnett B. A., Fan S., Moxim W. J., Levy H. II and Tilbrook B. (2007) The southern ocean biological response to aeolian iron deposition. *Science* **317**(5841), 1067–1070.

Chomchoei R., Miró M., Hansen E. H. and Shiowatana J. (2005) Automated Sequential Injection-Microcolumn Approach with On-Line Flame Atomic Absorption Spectrometric Detection for Implementing Metal Fractionation Schemes of Homogeneous and Nonhomogeneous Solid Samples of Environmental Interest. *Anal. Chem.* **77**(9), 2720-2726.

Cook H. E., Johnson P. D., Matti J. C. and Zemmels I. (1975) Methods of sample preparation and X-ray diffraction analysis in X-ray mineralogy laboratory. Kaneps, A.G., et al. (Eds.), Init. Repts DSDP. Print. Office, Washington, DC, p. 997–1007.

Cosentino N. J., Ruiz-Etcheverry L. A., Bia G. L., Simonella L. E., Coppo R., Torre G., Saraceno M., Tur V. M. and Gaiero D. M. (2020a) Does satellite chlorophyll-a respond to southernmost Patagonian dust? A multi-year, event-based approach. *J Geohys Res, B* **125**(12), e2020JG006073.

Cosentino N. J., Gaiero D. M., Torre G., Pasquini A. I., Coppo R., Arce J. M. and Vélez G. (2020b) Atmospheric dust dynamics in southern South America: A 14-year modern dust record in the loessic Pampean region. *The Holocene* **30**(4), 575-588.

Cosentino N. J., Gaiero D. M. and Lambert F. (2021) Present-day Patagonian dust emissions: Combining surface visibility, mass flux and reanalysis data. *J. Geohys. Res., A* **126**, e2020JD034459.

Crespi-Abril A. C., Soria G., De Cian A. and López-Moreno C. (2018) Roaring forties: An analysis of a decadal series of data of dust in Northern Patagonia. *Atmos. Environ.* **177**, 111–119.

Croot P. L. and Johansson M. (2000) Determination of iron speciation by cathodic stripping voltammetry in seawater using the competing ligand 2-(2-Thiazolylazo)-p-cresol (TAC). *Electroanalysis* **12**, 565–576.

Cutter G. A., Andersson P., Codispoti L., Croot P., François R., Lohan M., Obata H. and Rutgers van der Loeff M. (2010) Sampling and sample-handling protocols for GEOTRACES cruises. 2010 GEOTRACES Standards and Intercalibration Committee.

Cwiertny D. M., Young M. A. and Grassian V. H. (2008) Chemistry and photochemistry of mineral dust aerosol. *Annu. Rev. Phys. Chem.* **59**, 27-51.

Desboeufs K. V., Losno R., Vimeux F. and Cholbi S. (1999) The pH-dependent dissolution of wind-transported Saharan dust. *J. Geohys. Res., A* **104**(D17), 21287-21299.

Desboeufs K. V., Losno R. and Colin J. L. (2001) Factors influencing aerosol solubility during cloud processes. *Atmos. Environ.* **35**(20), 3529-3537.

Duggen S., Croot P., Schacht U. and Hoffmann L. (2007) Subduction zone volcanic ash can fertilize the surface ocean and stimulate phytoplankton growth: Evidence from biogeochemical experiments and satellite data. *Geophys. Res. Lett.* **34**(1).

Eggleton R. A. (1987) Noncrystalline Fe-Si-AI-Oxyhydroxides. *Clays. Clay. Miner.* ***35***(1), 29-37.

Erickson D. J. III, Hernandez J. L., Ginoux P., Gregg W. W., McClain C. and Christian J. (2003) Atmospheric iron delivery and surface ocean biological activity in the Southern Ocean and Patagonian region. *Geophys. Res. Lett.* **30**(12), 1609.

Fryrear D. W. (1986) A field dust sampler. *J. Soil Water Conserv*. **41**, 117–120.

Gaiero D. M., Probst J.-L., Depetris P. J., Bidart S. M. and Leleyter L. (2003) Iron and other transition metals in Patagonian riverborne and windborne materials: Geochemical control and transport to the southern South Atlantic Ocean. *Geochim. Cosmochim. Acta* **67(**19), 3603-3623.

Gaiero D. M., Depetris P. J., Probst J.-L., Bidart S. M. and Leleyter L. (2004) The signature of river- and wind-borne materials exported from Patagonia to the southern latitudes: a view from REEs and implications for paleoclimatic interpretations. *Earth Planet. Sci. Lett.* **219**(3–4), 357–376.

Gaiero D. M., Simonella L. E., Gassó S., Gili S., Stein A. F., Sosa P., Becchio R., Arce J. and Marelli H. (2013) Ground/satellite observations and atmospheric modeling of dust storms originating in the high Puna-Altiplano deserts (South America): Implications for the interpretation of paleo-climatic archives. *J. Geohys. Res., A* **118**, 1–15.

Gassó S. and Torres O. (2019) Temporal characterization of dust activity in the Central Patagonia desert (years 1964–2017). *J. Geohys. Res., A* **124**, 3417–3434.

Gassó S. and Stein A. F. (2007) Does dust from Patagonia reach the sub-Antarctic Atlantic Ocean? *Geophys Res Lett* **34**(1).

Gassó S., Stein A., Marino F., Castellano E., Udisti R. and Ceratto J. (2010) A combined observational and modeling approach to study modern dust transport from the Patagonia desert to East Antarctica. *Atmos. Chem. Phys.* **10**(17), 8287–8303.

Gili S., Gaiero D. M., Goldstein S. L., Chemale Jr F., Jweda J., Kaplan M. R., Becchio R. A. and Koester E. (2017) Glacial/interglacial changes of Southern Hemisphere wind circulation from the geochemistry of South American dust. *Earth Planet. Sci. Lett.* **469**, 98-109.

Hamilton D. S., Lee L. A., Pringle K. J., Reddington C. L., Spracklen D. V. and Carslaw K. S. (2014) Occurrence of pristine aerosol environments on a polluted planet. *PNAS* **111**(52), 18466-71.

Hand J. L., Mahowald N. M., Chen Y., Siefert R. L., Luo C., Subramaniam A. and Fung I. (2004) Estimates of atmospheric-processed soluble iron from observations and a global mineral aerosol model: Biogeochemical implications. *J. Geohys. Res., A* **109**(D17).

Hegg D. A., Gao S. and Jonsson H. (2002) Measurements of selected dicarboxylic acids in marine cloud water. *Atmos. Res.* **62**(1-2), 1-10.

Hepper E. N., Buschiazzo D. E., Hevia G. G., Urioste A. and Antón L. (2006) Clay mineralogy, cation exchange capacity and specific surface area of loess soils with different volcanic ash contents. *Geoderma* **135**, 216–223.

Hernández M. A., González N. and Hernández L. (2008) Late Cenozoic geohydrology of Extra-Andean Patagonia, Argentina. In J. Rabassa (Ed.), The Late Cenozoic of Patagonia and Tierra del Fuego (Vol. 11, pp. 497–509). Elsevier.

Ingall E. D., Feng Y., Longo A. F., Lai B., Shelley R. U., Landing W. M., Morton P. L., Nenes A., Mihalopoulos N., Violaki K., Gao Y., Sahai S. and Castorina E. (2018) Enhanced iron solubility at low pH in global aerosols. *Atmosphere* **9**(5), 201.

Ito A. and Feng Y. (2010) Role of dust alkalinity in acid mobilization of iron. *Atmos. Chem. Phys.* **10**(19), 9237-9250.

Jickells T. D. and Spokes L. J. (2001) Atmospheric iron inputs to the oceans. In: The Biogeochemistry of Iron in Seawater. Wiley, pp. 85-121.

Johnson M. S., Meskhidze N., Solmon F., Gassó S., Chuang P. Y., Gaiero D. M., Yantosca R. M., Wu S., Wang Y. and Carouge C. (2010) Modeling dust and soluble iron deposition to the South Atlantic Ocean. *J. Geohys. Res., A* **115**(D15).

Johnson M. S., Meskhidze N., Kiliyanpilakkil V. P. and Gasso S. (2011) Understanding the transport of Patagonian dust and its influence on marine biological activity in the South Atlantic Ocean. *Atmos. Chem. Phys.* **11**(6), 2487-2502.

Journet E., Desboeufs K. V., Caquineau S. and Colin J.-L. (2008) Mineralogy as a critical factor of dust iron solubility. *Geophys Res Lett* **35**(7).

Koffman B. G., Yoder M. F., Methven T., Hanschka L., Sears H. B., Saylor P. L. and Wallace K. L. (2021) Glacial dust surpasses both volcanic ash and desert dust in its iron fertilization potential. *Global Biogeochem. Cycles* **35**, e2020GB006821.

Kok J. F., Adebiyi A. A., Albani S., Balkanski Y., Checa-Garcia R., Chin M., Colarco P. R., Hamilton D. S., Huang Y., Ito A., Klose M., Li L., Mahowald N. M., Miller R. L., Obiso V., García-Pando C. P., Rocha-Lima A. and Wan J. S. (2021) Contribution of the world's main dust source regions to the global cycle of desert dust. *Atmos. Chem. Phys.* **21**(10), 8169-8193.

Lambert F., Opazo N., Ridgwell A., Winckler G., Lamy F., Shaffer G., Kohfeld K., Ohgaito R., Albani S. and Abe-Ouchi A. (2021) Regional patterns and temporal evolution of ocean iron fertilization and CO_2 drawdown during the last glacial termination. *Earth Planet. Sci. Lett.* **554**, 116675.

Li F., Ginoux P. and Ramaswamy V. (2008) Distribution, transport, and deposition of mineral dust in the Southern Ocean and Antarctica: Contribution of major sources. *J. Geohys. Res., A* **113**, D10207.

Mahowald N. M., Baker A. R., Bergametti G., Brooks N., Duce R. A., Jickells T. D., Kubilay N., Prospero J. M. and Tegen I. (2005) Atmospheric global dust cycle and iron inputs to the ocean. *Global Biogeochem. Cycles* **19**(4).

Marcotte A. R., Anbar A. D., Majestic B. J. and Herckes P. (2020) Mineral dust and iron solubility: Effects of composition, particle size, and surface area. *Atmosphere* **11**(5), 533.

Marino F., Castellano E., Ceccato D., De Deckker P., Delmonte B., Ghermandi G., Maggi V., Petit J. R., Revel-Rolland M. and Udisti R. (2008) Defining the geochemical composition of the EPICA Dome C ice core dust during the last glacial-interglacial cycle. *Geochem. Geophys. Geosyst.* **9**(10), Q10018.

Martin J. H. (1990) Glacial-interglacial CO_2 change: The iron hypothesis. P*aleoceanogr. Paleoclimatol.* **5**(1), 1–13.

Martin J. H., Gordon R. M. and Fitzwater S. E. (1990) Iron in Antarctic waters. *Nature* **345**(6271), 156-158.

Mingari L. A., Collini E. A., Folch A., Báez W., Bustos E., Osores M. S., Reckziegel F., Alexander P. and Viramonte J. G. (2017) Numerical simulations of windblown dust over complex terrain: the Fiambalá Basin episode in June 2015. *Atmos. Chem. Phys.* **17**(11), 6759-6778.

McCammon C. (1995). Mössbauer spectroscopy of minerals. In Mineral Physics & Crystallography, T. J. Ahrens (Ed.).

McLennan S. M. (1993) Weathering and global denudation. J. Geol. **101**(2), 295-303.

Meskhidze N., Chameides W. L., Nenes A. and Chen G. (2003) Iron mobilization in mineral dust: Can anthropogenic SO_2 emissions affect ocean productivity? *Geophys. Res. Lett.* **30**(21).

Meskhidze N., Nenes A., Chameides W. L., Luo C. and Mahowald N. (2007) Atlantic Southern Ocean productivity: Fertilization from above or below? *Global Biogeochem. Cycles* **21**(2).

Montes A., Rodríguez S. S. and Domínguez C. E. (2017) Geomorphology context and characterization of dunefields developed by the southern westerlies at drying Colhué Huapi shallow lake, Patagonia Argentina. *Aeolian Res.* **28**, 58–70.

Moore J. K., Doney S. C., Glover D. M. and Fung I. Y. (2001) Iron cycling and nutrient-limitation patterns in surface waters of the World Ocean. *Deep Sea Res. Part II* **49**(1–3), 463–507.

Murad E. (2010) Mössbauer spectroscopy of clays, soils and their mineral constituents. *Clay Minerals* **45**(4), 413-430.

Neff P. D. and Bertler N. A. (2015) Trajectory modeling of modern dust transport to the Southern Ocean and Antarctica. *J. Geohys. Res., A* **120**(18), 9303-9322.

Nesbitt H. and Young G. M. (1982) Early Proterozoic climates and plate motions inferred from major element chemistry of lutites. *Nature* **299**, 715-717.

Olgun N., Duggen S., Croot P. L., Delmelle P., Dietze H., Schacht U., Oskarsson N., Siebe C., Auer A. and Garbe-Schönberg D. (2011) Surface ocean iron fertilization: The role of airborne volcanic ash from subduction zone and hot spot volcanoes and related iron fluxes into the Pacific Ocean. *Glob. Biogeochem. Cycles* **25**, GB4001.

Orange D., Gac J.-Y., Probst J.-L. and Tanre D. (1990) Mesure du dépôt au sol des aérosols désertiques. Une méthode simple de prélèvement : le capteur pyramidal. *C. R. Acad. Sci.* **311**(2), 167–172.

Paris R. and Desboeufs K. V. (2013) Effect of atmospheric organic complexation on iron-bearing dust solubility. *Atmos. Chem. Phys.* **13**(9), 4895-4905.

Perron M. M., Strzelec M., Gault-Ringold M., Proemse B. C., Boyd P. W. and Bowie A. R. (2020) Assessment of leaching protocols to determine the solubility of trace metals in aerosols. *Talanta* **208**, 120377.

Placzek C., Quade J. and Patchett P. (2011) Isotopic tracers of paleohydrologic change in large lakes of the Bolivian Altiplano. *Quat. Res.* **75**(1), 231-244.

Poulton S. W. and Canfield D. E. (2005) Development of a sequential extraction procedure for iron: implications for iron partitioning in continentally derived particulates. *Chem. Geol.* **214**, 209-221.

Prospero J. M., Ginoux P., Torres O., Nicholson S. E. and Gill T. E. (2002) Environmental characterization of global sources of atmospheric soil dust identified with the Nimbus 7 Total Ozine Mapping Spectrometer (TOMS) absorbing aerosol product. *Rev. Geophys.* **40**(1), 2.1–2.31.

Pruppacher H. R. and Jaenicke R. (1995) The processing of water vapor and aerosols by atmospheric clouds, a global estimate. *Atmos. Res.* **38**(1-4), 283-295.

Raiswell R. and Canfield D. E. (2012) The iron biogeochemical cycle past and present. *Geochem. Perspect.* **1**(1), 1-220.

Rodríguez S., Prospero J. M., López-Darias J., García-Alvarez M. I., Zuidema P., Nava S., Lucarelli F., Gaston C. J., Galindo L. and Sosa E. (2021) Tracking the changes of iron solubility and air pollutants traces as African dust transits the Atlantic in the Saharan dust outbreaks. *Atmos. Environ.* **246**, 118092.

Romero M., Torre G. and Gaiero D. M. (2021) Paleoenvironmental changes in southern South American dust sources during the last glacial/interglacial transition: Evidence from clay mineral assemblages of the pampean loess. *Quat. Int.* **580**, 11-21.

Ryan P. C., Hillier S. and Wall A. J. (2008) Stepwise effects of the BCR sequential chemical extraction procedure on dissolution and metal release from common ferromagnesian clay minerals: A combined solution chemistry and X-ray powder diffraction study. *Sci. Total Environ.* **407**, 603-614.

Schroth A. W., Crusius J., Sholkovitz E. R. and Bostick B. C. (2009) Iron solubility driven by speciation in dust sources to the ocean. *Nat. Geosci.* **2**, 337–340.

Shelley R. U., Landing W. M., Ussher S. J., Planquette H. and Sarthou G. (2018) Regional trends in the fractional solubility of Fe and other metals from North Atlantic aerosols (GEOTRACES cruises GA01 and GA03) following a two-stage leach. *Biogeosciences* **15**(8), 2271-2288.

Shi Z., Bonneville S., Krom M. D., Carslaw K. S., Jickells T. D., Baker A. R. and Benning L. G. (2011a) Iron dissolution kinetics of mineral dust at low pH during simulated atmospheric processing. *Atmos. Chem. Phys.* **11**(3), 995–1007.

Shi Z. B., Woodhouse M. T., Carslaw K. S., Krom M. D., Mann G. W., Baker A. R., Savov I., Fones G. R., Brooks B., Drake N., Jickells T. D. and Benning L. G. (2011b) Minor effect of physical size sorting on iron solubility of transported mineral dust. *Atmos. Chem. Phys.* **11**(16), 8459-8469.

Shi Z., Krom M. D., Bonneville S., Baker A. R., Bristow C., Drake N., Mann G., Carlslaw K., McQuaid J. B., Jickells T. and Benning L. G. (2011c) Influence of chemical weathering and aging of iron oxides on the potential iron solubility of Saharan dust during simulated atmospheric processing. *Glob. Biogeochem. Cycles* **25**(2).

Shi Z, Krom M. D., Jickells T. D., Bonneville S., Carslaw K. S., Mihalopoulos N., Baker A. R. and Benning L. G. (2012) Impacts on iron solubility in the mineral dust by processes in the source region and the atmosphere: A review. *Aeolian Res.* **5**, 21-42.

Shoenfelt E. M., Sun J., Winckler G., Kaplan M. R., Borunda A. L., Farrell K. R., Moreno P. I., Gaiero D. M., Recasens C., Sambrotto R. N. and Bostick B. C. (2017) High particulate iron (II) content in glacially sourced dusts enhances productivity of a model diatom. *Sci. Adv.* **3**(6), e1700314.

Shoenfelt E. M., Winckler G., Lamy F., Anderson R. F. and Bostick B. C. (2018) Highly bioavailable dust-borne iron delivered to the Southern Ocean during glacial periods. *Proc.Nati. Acad. Sci.* **15**(44), 11180-11185.

Shoenfelt E. M., Winckler G., Annett A. L., Hendry K. R. and Bostick B. C. (2019) Physical weathering intensity controls bioavailable primary iron (II) silicate content in major global dust sources. *Geophys. Res. Lett.* **46**(19), 10,854–10,864.

Sholkovitz E. R., Sedwick P. N., Church T. M., Baker A. R. and Powell C. F. (2012) Fractional solubility of aerosol iron: Synthesis of a global-scale data set. *Geochim. Cosmochim. Acta* **89**, 173-189.

Simonella L. E., Gaiero D. M. and Palomeque M. E. (2014) Validation of a continuous flow method for the determination of soluble iron in atmospheric dust and volcanic ash. *Talanta* **128**, 248-253.

Simonella L. E., Palomeque M. E., Croot P. L., Stein A., Kupczewski M., Rosales A., Montes M. L., Colombo F., García M. G., Villarosa G. and Gaiero D. M. (2015) Soluble iron inputs to the Southern Ocean through recent andesitic to rhyolitic volcanic ash eruptions from the Patagonian Andes. *Glob. Biogeochem. Cycles* **29**, 1125–1144.

Song H., Marshall J., Follows M. J., Dutkiewicz S. and Forget G. (2016) Source waters for the highly productive Patagonian shelf in the southwestern Atlantic. *J. Mar. Syst.* **158**, 120–128.

Srinivas B., Sarin M. M. and Kumar A. (2012) Impact of anthropogenic sources on aerosol iron solubility over the Bay of Bengal and the Arabian Sea. *Biogeochemistry* **110**, 257-268.

Straub D. J., Lee T. and Collett Jr J. L. (2007) Chemical composition of marine stratocumulus clouds over the eastern Pacific Ocean. *J. Geophys. Res. Atmos.* **112**(D4).

Sudgen D. E., McCulloch R. D., Bory A. J.-M. and Hein A. S. (2009) Influence of Patagonian glaciers on Antarctic dust deposition during the last glacial period. *Nat. Geosci.* **2**, 281-285.

Taylor S. R. and McLennan S. M. (1985) The Continental Crust: Its Composition and Evolution, 312 pp., Blackwell Sci., Oxford.

Uno I., Eguchi K., Yumimoto K., Takemura T., Shimizu A., Uematsu M., Liu Z., Wang Z., Hara Y. and Sugimoto N. (2009) Asian dust transported one full circuit around the globe. *Nat. Geosci.* **2**(8), 557-560.

van Genuchten C. M., Rosing M. T., Hopwood M. J., Liu T., Krause J. and Meire L. (2021) Decoupling of particles and dissolved iron downstream of Greenlandic glacier outflows. *Earth Planet. Sci. Lett.* **576**, 117234.

Vergara-Jara M. J., Hopwood M. J., Browning T. J., Rapp I., Torres R., Reid B., Achterberg E. P. and Iriarte J. L. (2021) A mosaic of phytoplankton responses across Patagonia, the southeast Pacific and the southwest Atlantic to ash deposition and trace metal release from the Calbuco volcanic eruption in 2015. *Ocean Sci. J.* **17**(2), 561-578.

Villarreal M. L. and Coronato A. (2017) Characteristics and nature of pans in the semi-arid temperate/cold steppe of Tierra del Fuego. *In Advances in geomorphology and quaternary studies in Argentina* (pp. 203–224). Cham: Springer.

Wang P., Du Y., Yu W., Algeo T. J., Zhou Q., Xu Y., Qi L., Yuan L. and Pan W. (2020) The chemical index of alteration (CIA) as a proxy for climate change during glacial-interglacial transitions in Earth history. *Earth Sci. Rev.* **201**, 103032.

Wilson S. I. and Cooke R. V. (1980) *Wind Erosion in Soil Erosion.* John Wiley & Sons, New York, NY, pp. 217-251.

Yamamoto A., Abe-Ouchi A., Ohgaito R., Ito A. and Oka A. (2019) Glacial CO_2 decrease and deep-water deoxygenation by iron fertilization from glaciogenic dust. *Clim. Past* **15**, 981-996.

Zanbak C. and Arthur R. C. (1986) Geochemical and engineering aspects of anhydrite/gypsum phase transitions. *Bull. Assoc. Eng. Geol.* **23**(4), 419-433.

Zhu X., Prospero J. M., Millero F. J., Savoie D. L. and Brass G. W. (1992) The solubility of ferric ion in marine mineral aerosol solutions at ambient relative humidities. *Mar. Chem.* **38**(1-2), 91-107.

Declaration of interests

☒ The authors declare that they have no known competing financial interests or personal relationships that could have appeared to influence the work reported in this paper.

☐The authors declare the following financial interests/personal relationships which may be considered as potential competing interests: